Modelling, Simulation and Experimental Investigation of an Electrohydraulic Closed-Centre Power Steering System

Alessandro Dell'Amico, Petter Krus

Abstract—In steering-related active safety systems, active steering is a key component. Active steering refers to the possibility to control the road wheel angle or the required torque to turn the wheels by means of an electronic signal. Due to the high axle loads in heavy vehicles, hydraulic power is needed to assist the driver in turning the wheels. One solution to realise active steering is then to use electronically controlled valves that are of closed-centre type. This means that the assistance pressure, or force, can be set to any feasible value and still benefit from the high power density of fluid power systems. A closed-centre solution also implies that a significant reduction in fuel consumption is possible. This paper investigates such an electrohydraulic power steering system and a comparison with the original system is also made. The findings have shown that while a high response of the pressure control loop is desired for a good steering feel, instability might occur at higher steering wheel torque levels. This has effectively been shown and explained by simulation and hardware-in-the-loop simulation, together with linear analysis. For any desired boost curve, the response of the pressure control loop must be designed to preserve stability over the entire working range.

Index Terms—Active steering, power steering system, hardware-in-the-loop simulation, non-linear simulation

I. INTRODUCTION

AN ongoing trend in the vehicle industry is the development and implementation of active safety systems. Active safety systems are systems that provide assistance to the driver in more or less critical situations. Well established active safety systems include the Anti-lock Brake System and the Electronic Stability Program. This trend has also come to include the steering system, which relies on active steering. Active steering is the possibility to control the road wheel angle or the torque to turn the wheels by means of an electronic signal. Typical safety functions would assist the driver for example in avoiding a collision or unintended lane departures, [1], [2], [3]. Active steering is also useful in stabilising the vehicle and can complement the brakes, [4], [5], [6], [7]. Another system is the pedestrian safety system, where both brakes and steering are used to avoid collisions with pedestrians, [8]. Active steering is also a prerequisite when it comes to autonomous driving, [9], or steer-by-wire-systems, [10].

The purpose of the steering system in road vehicles is to provide the driver with a means to control the direction of the vehicle. With power steering, an assistive system is also

A. Dell'Amico and P. Krus are with the Division of Fluid and Mechatronic Systems, Linköping University, 58183 Linköping, Sweden (e-mail: alessandro.dellamico@liu.se; petter.krus@liu.se). Corresponding author: Alessandro Dell'Amico, (phone: +46 13 282732).

provided to reduce the drivers' work load when turning the road wheels. The traditional way of assisting the driver is by hydraulic power, the Hydraulic Power Assisted Steering (HPAS) system. A hydromechanical solution, comprising a rotational open-centre valve and a constant flow pump driven by the engine, controls the assistance pressure according to driver input. This system has reached a high level of acceptance due to its high power density, controllability, and reliability, [11]. This system also provides a good steering feel with its low inertia and friction. However, energy consumption is poor and it is not possible to implement active steering. The term steering feel is associated with the torque feedback to the driver that provides information regarding the road and tyre dynamics, [12], and can be defined from objective measures such as returnability, on-centre feel, linearity, torque stiffness and steering sensitivity.

The Electrohydraulic Power Assisted Steering (EHPAS) system was introduced to improve the energy consumption of power steering systems, [13]. Here the pump is driven by an electric motor, which means that the flow can be varied depending on the driving situation, for example the vehicle's speed. Compared to the conventional system, fuel savings of up to 0.2 l per 100 km have been reported, [14]. During non-steering, the motor speed is very low since no assistance is needed. A certain degree of motor speed is, however, necessary in many cases to provide assistance without significant lag, [15]. Other advantages of the system include improved packaging and the possibility to vary the level of assistance for different scenarios and in that way to some extent tune the steering feel. The accepted steering feel of hydraulic power steering is also retained with this system. One disadvantage of this kind of EHPAS system is that active steering cannot be implemented. The variation in assist level can, however, be used to stabilise the vehicle. This was shown in [16], where a tractor-trailer was stabilised by varying the assist level according to the rate of change of the articulation angle.

In another version of the EHPAS system, the open-centre rotational valve is replaced with a closed-centre rotational valve, [17], [18]. At centre position, the valve has closed ports between the pump and cylinder chambers. A small valve overlap provides a region of manual steer, improving steering feel and straight-line stability. A smaller pump can also be used since one flow path is no longer active during steering.

In the passenger car industry, the Electric Power Assisted Steering (EPAS) system has become very common. Here,

the hydraulic system is replaced with an electric motor that provides the level of assistance necessary either through the steering column or directly through the rack, [19]. The EPAS system only applies a torque when necessary and dramatically reduces energy consumption compared to the HPAS system, [20]. Challenges with the EPAS system have been the steering feel, which is compromised due to the high inertia of the electric motor, friction, backlash, and torque ripples. Another advantage of the EPAS system is that it permits active steering directly. The system is electronically controlled and the assistance torque can therefore be adapted to different safety functions.

When it comes to heavy vehicles, hydraulic power is still needed to assist the driver in turning the wheels due to the greater axle loads. The exception is hybrid vehicles where a high voltage battery allows the use of an EPAS system. In [21], the energy recovery potential of the EPAS system was investigated for a hybrid bus, where up to 20% of the energy needed to complete a full steering manoeuvre could be recovered. One way to realise active steering in hydraulic power steering systems is described in [22]. An electric motor acts through a planetary gear and can increase or decrease the road wheel angle applied by the driver. Another solution is the Active Pinion concept, [23]. An actuator affects the hydraulic valve directly, modifying the relation between the driver's torque and the assistance torque, and an offset torque can be produced. The actuator can be a small electric motor. A solution for heavy vehicles is presented in [24]. An electric motor acts on the steering column and works through the hydraulic system. The system is referred to as hybrid steering. For low demands, the assistance is provided by the electric motor. For higher demands, the hydraulic system also provides the necessary assistance. Two torque measurements are needed: one for the hydraulic system and one for the electric system. By controlling the pump flow, the energy consumption can be reduced by up to 80% compared to the HPAS system depending on driving scenario. Active steering is also possible. A similar system was modelled and controlled in [9], where the objective was autonomous driving.

A solution that addresses both the energy consumption and active steering is another type of electrohydraulic power steering system, where electronically controlled closed-centre valves are used, which is studied and discussed in [25] and [26]. This solution takes advantage of the high power density of fluid power systems and the good steering feel and provides a compact solution. In addition, only one torque measurement is needed. The system relies on constant pressure instead of constant flow. An accumulator can provide peak flow demands, which allows the pump to be made smaller. Proper design and control of the valves is needed to ensure stability and good tracking. Measurements from a driving cycle, similar to the New European Driving Cycle, shows that the closed-centre system only uses 18% of the energy consumed by the original open-centre hydraulic system.

The contribution of this paper is an analysis of such an electrohydraulic power steering system with closed-centre valves, which is a highly interesting solution for the heavy vehicle industry for the reasons mentioned above. The analysis
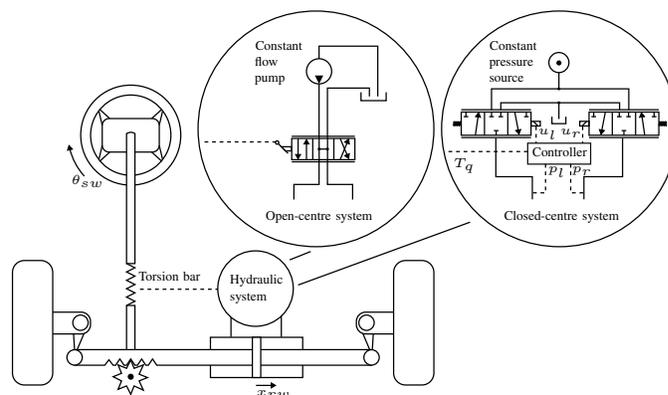

Fig. 1. A schematic of the steering system showing, both the open-centre and closed-centre hydraulic systems.

is made in both the frequency domain and the time domain with the focus on stability and performance. Both a new linear model and a non-linear model are derived for this purpose. In this way, analytical expressions for stability properties have been derived.

In this work only, high performance servo valves represent the closed-centre circuit. It can be seen as a generalised solution, although not a feasible one due to the high cost, but nonetheless serves to analyse the system. The procedure and results of this work are applicable to any configuration of such a system. A test rig has also been developed for hardware-in-the-loop simulation and is used to confirm findings and provide a measure to validate the models. A comparison of the original open-centre system is also provided to better describe what challenges the closed-centre system involves.

The linearised model is used to show how the pressure loop dynamics relate to the steering system loop dynamics, when and why instability occurs, and what design aspects of the pressure actuator there are to consider. These results are then also verified with the help of the validated simulation model, as well as they are shown in the test rig. The results are useful when designing the system characteristic or any necessary controllers for such an electrohydraulic power steering system.

The paper is organised as follows. Section II describes both the reference open-centre system and the closed-centre system under study and the test rig. All modelling is presented in section III, together with a review of the existing literature in the field. The control strategy is explained in section IV and in section V the systems are analysed in the frequency domain. Section VI describes the simulation procedures. The results are presented in section VII and a discussion and the conclusions from the study can be found in sections VIII and IX, respectively.

II. SYSTEM DESCRIPTION

The power steering system is a position control system, where the driver controls the steering wheel angle. This represents the reference position and the power steering system controls the road wheel angle and aims to follow the reference. The closed-centre system is compared to the original system from a dynamics perspective. This is to better understand
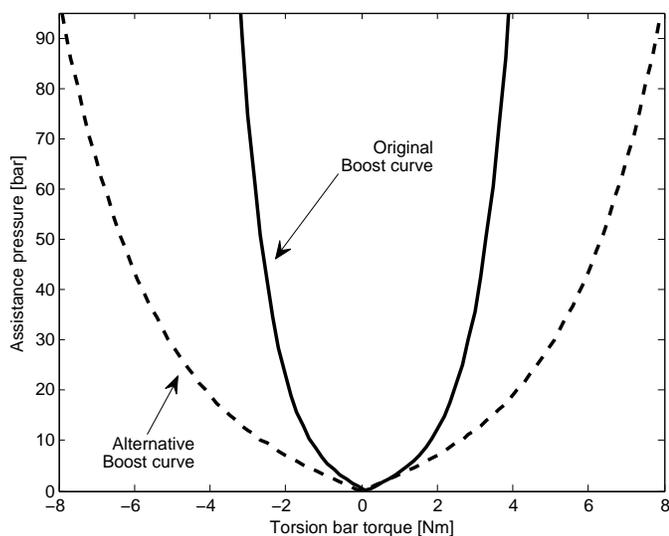
Fig. 2. The solid line shows the boost curve of the original system, measured from the test rig. The dashed line shows an alternative boost curve used for comparison with the original curve when controlling the closed-centre system.

the fundamental differences between these systems and what challenges the closed-centre system involves. The systems modelled and studied are identical to the systems in the test rig, as described below. This is to facilitate the comparison between simulation and testing. This section describes both the open-centre and closed-centre systems and the test rig. A schematic of both systems is shown in Fig. 1, where the fundamental difference in hardware set-up is distinguished.

A. Open-centre hydraulic power steering system

The traditional power steering system is made up of a constant flow pump, driven by the engine, and a rotational open-centre valve. The valve is mechanically connected to a torsion bar and is activated by the twisting of the torsion bar, i.e. the driver input torque. When the valve is twisted, the control edges on one side are closed and opened at the other, increasing the pressure on the closing side, and an assistive force is created. The pressure is also very much dependent on the pump flow. This effectively means that the hydraulic system is a pressure control system, which is an inherent property of an open-centre system.

The system is dimensioned for the heaviest load case. This occurs during parking manoeuvres, where the required assistive force is high, while the pump speed is low. During high-speed driving, the need for assistance is instead low, while the pump speed is high. A substantial amount of oil is then fed back to tank and together with the open-centre valve this is the reason for the open-centre system's poor energy efficiency.

The power steering system is characterised by the boost curve, which defines the assistive pressure for a given torsion bar torque. In the open-centre system, the boost curve is defined by the geometry of the valve and the pump flow. The measured boost curve of the test rig is shown in Fig. 2, with a pump flow of 9 l/min.
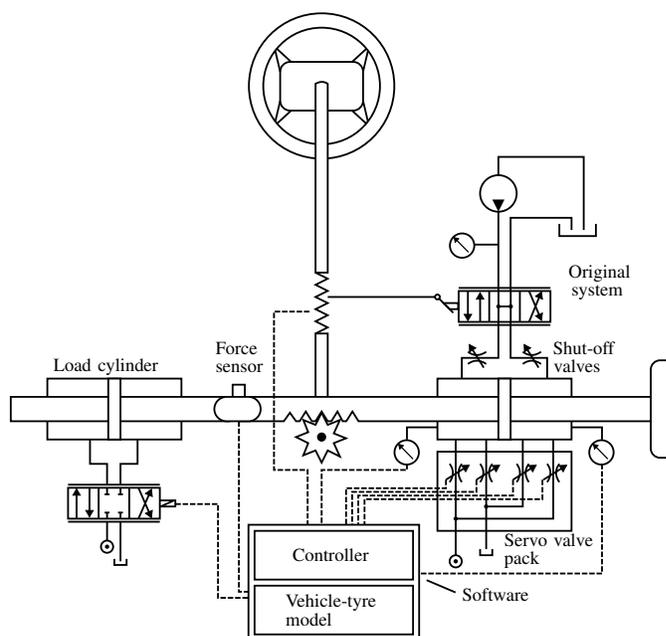

Fig. 3. Schematic representation of the test rig. The shut-off valves allow switching between the original and the closed-centre system. The software contains the controller for the servo valves as well as a vehicle-tyre model to represent the force exerted on the rack.

B. Closed-centre electrohydraulic power steering system

The open-centre valve is replaced by electronically controlled closed-centre valves that individually control the pressure in each chamber of the assistance cylinder. Different solutions are possible here, e.g. proportional directional valves or pressure control valves, [26]. In this work, high-performance servo valves are used as a case example. They are only intended for experimental testing and serve as a benchmark. There is no mechanical connection to the torsion bar as in the open-centre case, but control of the valves relies instead on measurement of the torque. The supply to the servo valves is a constant pressure system.

One of the requirements of such a closed-centre system is a different supply system compared to the original system. This opens up for further improvements, e.g. as regards packaging and energy consumption. Extensive research findings have been reported, e.g. in [27], but this area is beyond the scope of this work.

C. Test rig

The test rig, illustrated in Fig. 3, is built around a rack-and-pinion steering system. The original system is retained as reference system. Parallel to the original system is the closed-centre electrohydraulic system, which uses the same mechanical structure. Manual shut-off valves are used to switch between the two systems. A load cylinder is attached to the rack that applies a force according to a software-implemented vehicle-tyre model. A force sensor is used to measure the rack load. At the other end, a mass is attached, contributing the system inertia. The rig is also equipped with a rack position sensor, a steering wheel angle sensor and pump

and load pressure sensors. The torsion bar is also used as a torque sensor by attaching strain gauges. This eliminates the need for an extra torsion bar. The rack's velocity is derived by differentiating the rack position.

As mentioned previously, for the purposes of the investigations in this study, four high-performance servo valves are used to represent an electrohydraulic closed-centre solution. These valves do not represent a feasible solution for the final application, mainly due to their high price, but they do give an indication of the level of performance needed and a certain degree of flexibility during testing. For individual control of the pressure in each chamber, at least two valves are needed. With four valves, the meter-in and meter-out flow of each chamber can be controlled individually. This functionality is not used here but could be useful in future experiments. A laboratory set-up is used to supply a constant pressure.

III. SYSTEM MODELLING

Non-linear models are derived for both the open-centre and the closed-centre system. These models are used for simulation and stability analysis. The latter requires a linearisation of the system equations. The two systems share the same mechanical subsystem.

A. Mechanical subsystem

The model's level of complexity is very much related to its purpose and a great deal of research has been done on the subject. Too complex a model will increase computational time and be more difficult to analyse. In [28], a 5 DoF and a 2 DoF model were developed for the mechanical subsystem and compared to measurements. The simpler model performs sufficiently well to study the behaviour of the steering wheel torque. In [29], a 2 DoF model was derived for a passenger car and a 3 DoF model for a truck. In [30], a 3 DoF model was developed and the importance of non-linear effects, such as friction and boost pressure, was shown. In [31], the choice was a 2 DoF model for the mechanical structure, with the purpose of analysing stability in the frequency domain of an EPAS system. The purpose of the present model is to study the steering wheel torque and stability, and since the application is the test rig without wheel assembly, a 2 DoF model of the mechanical subsystem is chosen.

The steering wheel and column constitute the upper inertia, J_{sw}, and the rack with mass constitutes a translational mass, M_{rw}, as shown in (1) and (2). Steering wheel torque is denoted T_{sw}, stiffness K_t, steering gear ratio R_t, viscous friction coefficient b, load stiffness C_{rw}, and cylinder area A_p. The steering wheel is denoted with index sw and the road wheels, or the rack in this case, are denoted with index rw. The load pressure is denoted p_L and is defined as the difference between the right and left cylinder chambers, $p_L = p_{right} - p_{left}$. The friction is an important parameter for proper behaviour of the model and in [32], a spring/friction model is suggested. A static friction is used for the column, denoted F_f, and a pressure-dependent friction for the rack, $F_{f,p}(p_L)$. A spring/hysteresis model is adapted for this purpose. Definitions of the steering wheel angle θ_{sw} and the rack position x_{rw} are shown in Fig. 1.
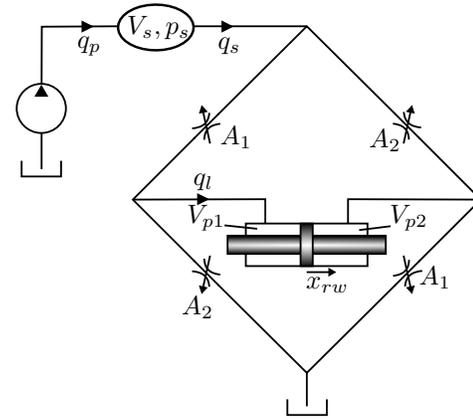

Fig. 4. Schematic representation of the open-centre system.

Parameters needed for the model, such as friction levels and stiffness, are measured on the test rig, as described in [33], where also intial parts of the modelling procedure is presented.

$$J_{sw}\ddot{\theta}_{sw} = T_{sw} - K_t(\theta_{sw} - x_{rw}R_t) - b_{sw}\dot{\theta}_{sw} - F_f \quad (1)$$

$$M_{rw}\ddot{x}_{rw} = p_L A_p + K_t(\theta_{sw} - x_{rw}R_t)R_t - b_{rw}\dot{x}_{rw}$$
$$- C_{rw}x_{rw} - F_{f,p}(p_L) \quad (2)$$

The linearisation of the mechanical subsystem can be found in the appendix.

B. Open-centre system

The open-centre valve consists of several control edges but is preferably modelled as a lumped Wheatstone bridge, as shown in Fig. 4, with opposite orifices assumed to be equal. This has proven to be useful, [34]. Modelling and analysis of the open-centre valve can be found in [35]. The system flow q_s and the load flow q_l are described by (3) and (4), with flow coefficient C_q, oil density ρ and system pressure p_s. Statically, the system flow is equal to the pump flow q_p.

$$q_s = C_q A_1\sqrt{\frac{p_s - p_L}{\rho}} + C_q A_2\sqrt{\frac{p_s + p_L}{\rho}} \quad (3)$$

$$q_l = C_q A_1\sqrt{\frac{p_s - p_L}{\rho}} - C_q A_2\sqrt{\frac{p_s + p_L}{\rho}} \quad (4)$$

The opening areas A_1 and A_2 are derived from the measured boost curve. The static load pressure is shown in (5), derived from (3) and (4), with $A_2 = A[T_{sw}]$ and $A_1 = A[-T_{sw}]$, and is an analytical expression of the boost curve and is used to calculate the reference pressure, which will be explained later. The flow ratio is defined as $q = \frac{q_l}{q_p}$.

$$p_L(T_{sw}, q) = \frac{\rho q_s^2}{8C_q^2}\left(\left(\frac{1-q}{A[T_{sw}]}\right)^2 - \left(\frac{1+q}{A[-T_{sw}]}\right)^2\right) \quad (5)$$

The pressure built up in the system volume V_s and load volume $V_0 = \frac{V_{p1}V_{p2}}{V_{p1}+V_{p2}}$ is shown in (6) and (7), with bulk modulus β.

$$q_p - q_s = \frac{V_s}{\beta}\dot{p}_s \quad (6)$$

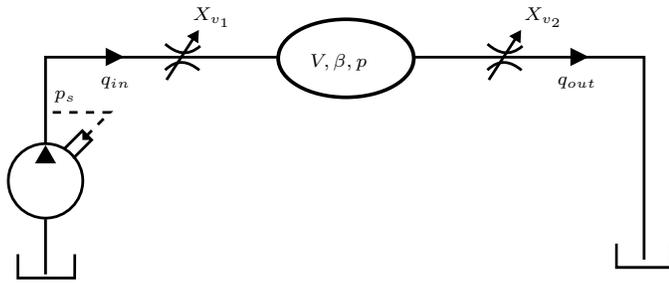$$q_l = A_p\dot{x}_{rw} + \frac{V_0}{\beta}\dot{p}_L \quad (7)$$

Fig. 5. Representation of the pressure control with servo valves for one chamber.
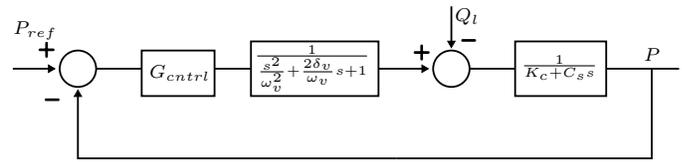

Fig. 6. Block diagram representation of the pressure control loop of the closed-centre system, from reference pressure P_{ref} to actual pressure P.

From the linearised equations, as shown in the appendix, the transfer function for the load pressure can be solved as shown in (8).

$$
P_L = \frac{K_{c1}}{K_{c1}^2 - K_{c2}^2} \frac{1 + \frac{V_s}{K_{c1}\beta}s}{\frac{s^2}{\omega_0^2} + \frac{2\delta_0}{\omega_0}s + 1} \cdot
$$
$$
\left(\frac{1 + \frac{V_s}{\left(K_{c1} + \frac{K_{q2}K_{c2}}{K_{q1}}\right)\beta}s}{1 + \frac{V_s}{K_{c1}\beta}s} K_{q1} \left(1 + \frac{K_{q2}K_{c2}}{K_{q1}K_{c1}}\right) T_{sw} \right.
$$
$$
\left. - A_p X_p s \right)
$$
$$
\approx \frac{G_{K_c}(s)}{K_c} \left(G_{K_q}(s) K_q T_{sw} - A_p X_p s \right) \tag{8}
$$

The coefficients are defined in the appendix. The pressure response is mainly dominated by a first order dynamics, especially for the low-torque region and for the low-frequency region at higher torque levels. This is also shown in Fig. 8.

C. Closed-centre system

Modelling and analysis of the closed-centre valve can be found in [35]. Since the pressure is controlled independently in each chamber, studying the pressure response in one chamber is sufficient. The system is illustrated in Fig. 5. It is assumed that supply pressure p_s is maintained at a constant level. The system of equations is shown in (9) to (11), with parameters defined in Fig. 5.

$$
q_{in} = C_q w x_{v1} \sqrt{\frac{2}{\rho} (p_s - p)} \tag{9}
$$

$$
q_{out} = C_q w x_{v2} \sqrt{\frac{2}{\rho} p} \tag{10}
$$

$$
q_{in} - q_{out} = A_p \dot{x}_{rw} + \frac{V}{\beta} \dot{p} \tag{11}
$$

A feedback loop of the spool position with PI controller and a second order dynamics are used to generate the valve opening and better correspond to measurements of the pressure, shown in section VII. For linear analysis, the valve opening is assumed to have only a second order dynamics, as shown in (12), with resonance frequency ω_v and damping δ_v. The meter-in and meter-out valves are controlled simultaneously, as shown in (28) in the appendix, which results in higher system gain. The linearisation of the system can be found in the appendix.

$$
X_v = \frac{X_{v_{ref}}}{\frac{s^2}{\omega_v^2} + 2\frac{\delta_v}{\omega_v}s + 1} \tag{12}
$$

IV. CONTROL

While control of the pressure for the open-centre system is purely hydromechanical, controlled by the twisting of the torsion bar via the boost curve, the closed-centre system relies on a software-implemented controller and boost curve. In order to control the static characteristic, the controller needs to be of integrator type. The valve dynamics also introduces a fair degree of phase shift and in order to compensate for this a derivative part is also introduced to the controller. The system is strongly non-linear and for improved performance, the controller is adaptive in that it compensates for varying system dynamics, seen from (29). The controller is implemented as a lead-lag filter as shown in (13), taking the difference between the reference pressure and measured pressure as input. A similar approach was used in [36].

$$
G_{cntrl}(s) = \frac{K_{p0}}{\hat{K}_q} \left(\frac{\frac{V}{\beta \hat{K}_c}s + 1}{\frac{V}{\beta \hat{K}_c}s + \gamma} \right) \left(\frac{\frac{1}{\omega_v}s + 1}{\frac{\alpha}{\omega}s + 1} \right) \tag{13}
$$

The estimated system variables $\hat{K}_q$ and $\hat{K}_c$ are calculated according to the expression shown in (30) to (35), and γ and α are tuned for good performance. In the subsequent analyses, it is assumed that $\hat{K}_q$ and $\hat{K}_c$ are perfectly estimated. With (29), (12) and (13), the pressure control loop for the closed-centre system can be derived in the block diagram shown in Fig. 6. This loop constitutes the inner control loop of the power steering system, as will be shown.

As in the case of the open-centre system, the reference pressure for the closed-centre system is defined by the boost curve. This is the most common way to control the pressure. For a comparison to be valid, it is also necessary to control the closed-centre system in a similar fashion. The reference pressure on a linear form is expressed as shown in (14), with $K_{q_{OC}}$ and $K_{c_{OC}}$ being the flow gain and flow-pressure coefficient for the open-centre system, respectively. A pre-filter is also applied to shape the response. Two cases are evaluated. One is a pre-filter generating open-centre dynamics, the other with a low-pass filter with 50 Hz break frequency. For good performance in the test rig, the mean pressure was raised by 50 bar in each cylinder. This does not affect the assistance pressure, but might generate more friction.

$$
P_{ref} = G_{filter}(s) \frac{1}{K_{c_{OC}}} \left(K_{q_{OC}} \left(\theta_{sw} - R_T X_{rw} \right) K_T \right.
$$
$$
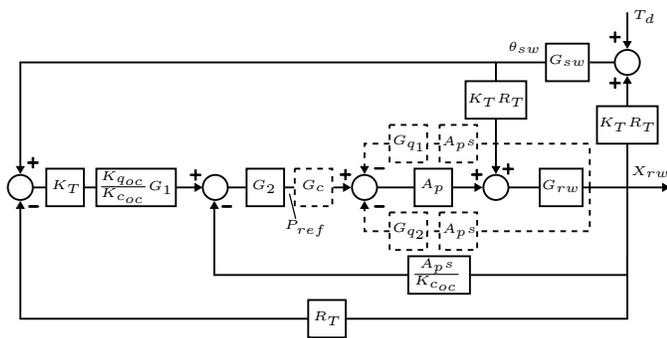\left. - A_p X_{rw} s \right) \tag{14}
$$

Fig. 7. Block diagram representation of the power steering system. The dashed lines are for the closed-centre system only.
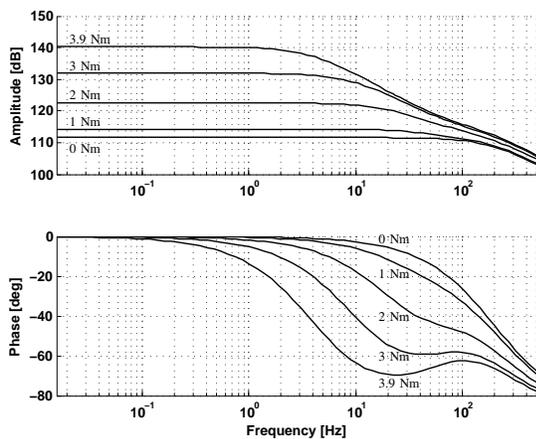

Fig. 8. Frequency plot of the pressure response for the open-centre system. The different lines correspond to different torque levels.
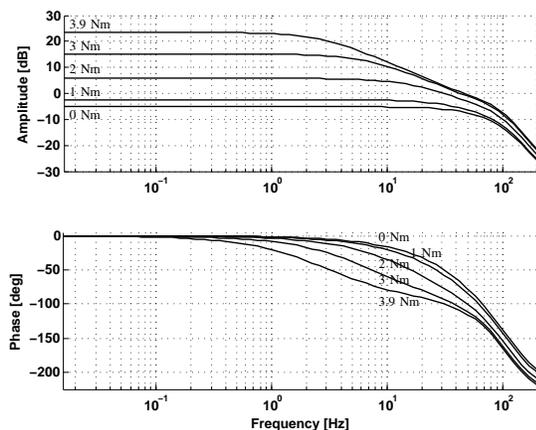

Fig. 9. Frequency plot of the open loop of the open-centre power steering system. The different lines correspond to different torque levels.

V. SYSTEM ANALYSIS

Both systems are analysed with the help of the derived linear models in order to study and compare their respective behaviour. Parameter values used in this work are as shown in Table I in the appendix.

A. Open-centre system

A block diagram of the original system, shown in Fig. 7, can be derived with (17), (18) and (8). In this case the
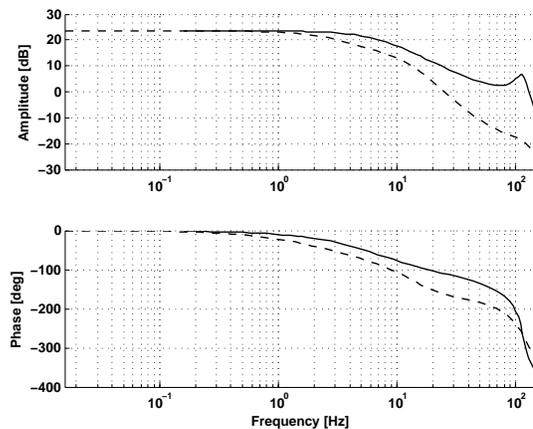

Fig. 10. Frequency plot of the open loop of the closed-centre power steering system. Solid curve represents with a pre-filter at 50 Hz, and dashed curve represents with a pre-filter with open-centre dynamics.

transfer function $G_1(s) = G_{K_q}(s)$ and $G_2(s) = G_{K_c}(s)$, as defined in (8). The mechanical transfer functions of the steering wheel and rack are denoted $G_{sw}(s)$ and $G_{rw}(s)$, respectively, and are defined in the appendix. The dashed blocks and lines are valid only for the closed-centre system, as will be described later. The block diagram shows the closed loop system, where the steering wheel angle is the reference signal and the corresponding rack position is fed back. Improper design might lead to instability problems. Stability margins can be seen from frequency analysis of the system.

Due to the non-linear behaviour of the system, several operating points need to be studied. Since both the area opening of the valve and the pressure level are set by the torque, the system is studied for different torque levels, as well as different load flow levels. Figure 8 shows the frequency analysis of the pressure response of the original system for zero load flow and with the steering wheel in the centre position. Higher torque leads to higher gain but also a significantly slower system. The effect of this is seen in the frequency analysis of the open loop system, from a steering wheel angle to rack position, shown in Fig. 9. The stability margin is mainly set by the amplitude margin. The increase in gain with increased torque leads to a reduced amplitude margin. This is compensated for by the slower dynamics of the pressure response, where an increase in the amplitude margin is reset. The dynamics of the pressure response are defined by the geometry of the valve, as is also the steady state gain, or boost gain. This means that there is a fixed relation between the boost gain and the system's bandwidth.

B. Closed-centre system

Since the closed-centre system is controlled in a similar fashion to the open-centre system, the block diagram will have a similar appearance, as shown in Fig. 7. Depending on the choice of pre-filter, $G_1(s)$ and $G_2(s)$ will look different. For open-centre dynamics, they will be equal, as in the open-centre system. For the case with fixed pre-filter, $G_1(s) = 1$ and $G_2(s) = \frac{1}{1+\frac{s}{\omega_b}}$. The additional dynamics come from

the pressure response. From the block diagram in Fig. 6, the open loop and closed loop of the pressure response with the servo valves can be derived and are shown in (15) and (16), respectively.

$$G_o(s) = \frac{G_{cntrl}(s)}{\left(\frac{s^2}{\omega_v^2} + \frac{2\delta_v}{\omega_v}s + 1\right)(K_c + C_s s)} \tag{15}$$

$$P_L = P_{right} - P_{left} = \underbrace{\frac{G_o}{1 + G_o}}_{G_c} P_{ref}$$

$$- \left(\underbrace{\frac{1}{(K_c + C_s s)(1 + G_o)}}_{\text{right chamber, } = G_{q_1}} + \underbrace{\frac{1}{(K_c + C_s s)(1 + G_o)}}_{\text{left chamber, } = G_{q_2}}\right) Q_l \tag{16}$$

The frequency analysis of the open loop of the closed-centre power steering system is shown in Fig. 10 for zero load flow and with the steering wheel in the centre position. The two cases are shown for the highest torque level, which corresponds to the highest gain level. In the first case, with dashed line, the pre-filter of the controller has the same first order dynamics as the open-centre valve. This results in a positive amplitude margin and a stable system. In the second case, the pre-filter is set at 50 Hz, which is much higher than the first case. This results in a negative amplitude margin and an unstable system. This illustrates the main difference compared to the open-centre system. There is no relation between the gain and the bandwidth of the pressure response and too high a bandwidth will reduce the amplitude margin.

VI. SIMULATION

Simulation has been a valuable tool in understanding the closed-centre power steering system and provides a means to test different set-ups of the system, as well as develop control strategies. Given the strongly non-linear nature of fluid power systems, simulation is also an effective tool to test the system over the entire working range. The aim has been to verify the behaviour seen from the linear analysis, namely that too high a bandwidth of the pressure control loop might lead to instability at high pressure levels for boost curve control. As part of the process of verifying and understanding the system, hardware-in-the-loop simulation has also been a valuable tool. With hardware-in-the-loop simulation, part of the system consists of the actual hardware and the other part as simulation models implemented in a real-time computer. Examples of hardware-in-the-loop simulation test rigs and how they are used can be found for example in [37].

Simulation models are always a reflection of real systems and simplifying the system is part of the process. With the actual hardware in place, the effect of different properties that were excluded in the pure simulation can also be studied. One advantage of a test rig is that it also provides a clear boundary of the system studied, which makes it easier to study the system and develop a model. In this case, it is also easier to mount sensors and test parts of the system for

model parametrisation than it would if they were installed in the actual application.

A. Computer simulation

The simulation model is divided into sub-models. A mechanical sub-model communicates with a hydraulic sub-model. A driver model is implemented as a PID controller that applies a torque to the mechanical sub-model in order to follow the measured steering wheel angle. The load cylinder with servo valve and controller is implemented for better resemblance to the test rig. The reference value comes from a spring load model. It can be seen as a tyre model during parking manoeuvres and is used to ensure that the steering system reaches maximum pressure. All equations are discretized with the Bilinear Transform and implemented with the Transmission Line Modelling method, [38]. This means that the same models can be used during hardware-in-the-loop simulation as well.

B. Hardware-in-the-loop simulation

The hardware consists of the rack-and-pinion system with steering wheel. The load cylinder attached to the rack is controlled by a servo valve to keep a certain force applied to the rack. The reference force is calculated from either a vehicle model or, as in this case, a spring model that takes the measured rack position as input. The lead-lag controller takes the difference between the reference and measured forces to calculate the control signal to the servo valve. A mass is attached at the other end of the rack to provide the inertia of the system. The load cylinder then only needs to provide the static load from the tyre-ground interaction. A sample time of 10 kHz was used. More on the control of the test rig can be found in [33].

VII. RESULTS

Figure 11 shows the responses of the pressure steps for the two different pre-filters used as well as without pre-filter. The top plot is without pre-filter. A high gain is chosen, which generates some oscillations. This is compensated for with the pre-filter, as shown in the bottom plot. The faster curves are with pre-filter at 50 Hz and the slower curves with open-centre dynamics as pre-filter. The model, shown as dashed lines, is able to predict the behaviour of the pressure loop sufficiently well compared to measured results, shown as solid lines. The figure also shows the reference curves for each case, shown as dashed-dotted lines. There is a clear difference in bandwidth between the two cases with pre-filter. The time lag between the reference and actual pressure is not of importance here, but merely illustrates the time lag introduced by the valves.

Figure 12 shows a comparison between the test rig and a simulated model of the rig for the open-centre system and closed-centre system with three cases. Figure 12a shows the assistive pressure, with a solid curve for measurement and a dashed curve for simulated results. Figure 12b shows the measured and simulated torsion bar torque. The top plots are for the open-centre system. The second top plots are for the
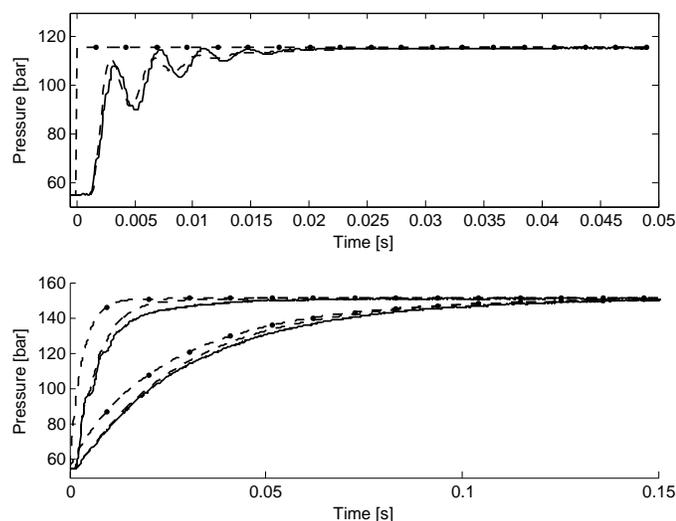
Fig. 11. Comparison between measured (solid) and simulated (dashed) pressure responses. The dashed-dotted line is the reference pressure for respective case. In the top plot, the pressure response without pre-filter is shown. The lower plot shows the pressure response with pre-filter, where the faster curves represent the 50 Hz pre-filter and the slower curves the dynamic open-centre model as pre-filter.

closed-centre system with open-centre dynamics as pre-filter and the system is stable. The third top plots are for the system with 50 Hz pre-filter. As the pressure increases, instability finally occurs and the system returns to a stable state as the pressure decreases again. The lower plots are the closed-centre system with 50 Hz pre-filter and the flatter boost curve, shown as an alternative boost curve in Fig. 2. The steering wheel angle was manually applied with an amplitude of 22-25°and no faster than 150°/s. In all cases, the simulation results also show the same behaviour.

VIII. DISCUSSION

Besides the fact that the open-centre system is hydrome-chanical while the closed-centre system, in this work, is electrohydraulic, there are two main differences between the two systems. The first is the relation between actuator dynamics and gain. For the open-centre system, both the gain and the bandwidth are defined by the boost curve, i.e. the geometry of the valve. Since the closed-centre system is electrohydraulic, the boost curve is implemented in the software and is separated from the valve dynamics. Intuitively, a fast pressure response is desired for a good steering feel, but as the gain increases with increased torque level the amplitude margin of the outer power steering loop is decreased. The bandwidth of the pressure response also affects the amplitude margin and too high a bandwidth might reduce it to such an extent that instability might occur. A slower bandwidth will therefore compensate for the smaller amplitude margin as the gain increases. This was seen from the linear analysis, where too high a bandwidth of the pressure control loop significantly reduced the amplitude margin. The same behaviour is also seen from the results in Fig. 12. In the second and third top plots the system is controlled with the same static boost curve but different pressure loop dynamics. The third top plots clearly show the

result from the unstable system with oscillations in pressure, Fig. 12a, as well as the torsion bar torque, Fig. 12b. The lower plots in Fig. 12 also show that the pressure loop dynamics must be designed for the chosen boost curve of the system. The flatter curve shown in Fig. 2 generates a lower boost gain and a faster response of the pressure control loop is therefore possible. The flatter boost curve used here also provided less damping, i.e. the change in pressure with change in load flow. In all cases, the simulation results are in good agreement with the measurements, although the rig shows slightly more oscillations.

The other main difference between the two systems is the additional lag introduced by the closed-centre valve. The hydromechanical solution of the open-centre valve means that the pressure is directly affected by the change in opening area, i.e. the twisting of the torsion bar. The closed-centre valve is not connected to the torsion bar mechanically and a change in pressure requires a change in flow, which in turn requires a change in valve position. The additional lag might have a negative impact on steering feel and a fast valve is therefore needed. This is not a concern at low torque levels, where the steering feel is most apparent, since the boost gain is low. The additional lag might also cause instability problems and a fast valve is therefore also desirable from that point of view.

The top plots in Fig. 12 illustrate the reference system and its behaviour. Some differences in behaviour between the top and second top plots are visible, especially in the torsion bar torque. This is mainly due to the fact that the additional phase shift from various parts of the system, as mentioned previously, can cause instability problems. The additional phase shift comes from the servo valves and filtered signals, such as rack position and velocity. The rack position is used to calculate the load and the velocity is used to calculate the right amount of assistive pressure to be applied. This could be improved on by using better sensors that require less filtering. Fig. 11 illustrates the additional phase shift from the pressure response of the closed-centre system compared to the original system. The model is also predicting the same behaviour. Another reason for the difference between the two top plots might be the higher friction in the assistance cylinder due to the higher mean pressure in this case, as described previously.

Good performance of the steering system is achieved by means of fast valves and controlling the response of the pressure control loop with the pre-filter.

IX. CONCLUSIONS

The linear analysis of the two systems has shown that, for the open-centre system both the bandwidth of the pressure response and the gain are related to the boost curve. The gain and bandwidth have a fixed relation, where the bandwidth decreases with increasing gain. This is in contrast to the closed-centre system, where the bandwidth of the pressure response is independent of the boost gain. With increased boost gain, the amplitude margin of the steering system loop decreases. Too high a bandwidth of the pressure loop might then result in instability.

Decreasing the bandwidth as the gain increases compensates for the loss in amplitude margin. This is also a property of the
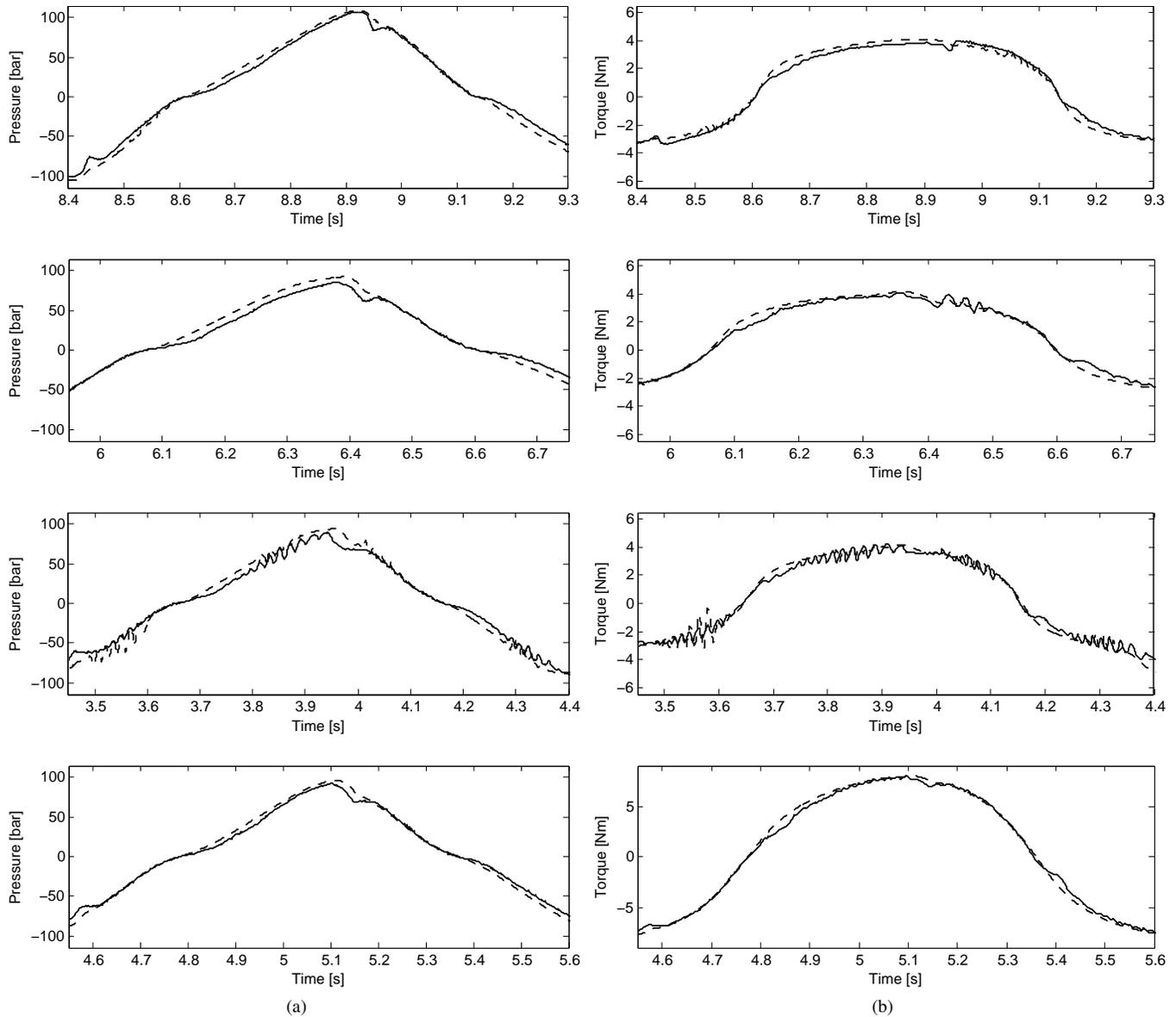
Fig. 12. Comparison between measured (solid) and simulated (dashed) pressure (a) and torsion bar torque (b). The top plots are the open-centre system while the other plots are the closed-centre system. The second top plots are with open-centre dynamics as pre-filter. The third top plots are with 50 Hz pre-filter. The bottom plots are with 50 Hz pre-filter and flat boost curve.

open-centre system. Simulation results have also shown this behaviour. A pre-filter is used to shape the desired pressure loop response. A 50 Hz first order pre-filter resulted in heavy oscillations as the pressure reached a higher level. By instead using open-centre dynamics as pre-filter, the system is stable. A flatter boost curve together with the 50 Hz pre-filter has also shown a more robust behaviour, verifying the relation between system stability, boost gain and pressure loop response. Hardware-in-the-loop simulation has also verified the same behaviour and simulation and measurements show good agreement, which confirms the theory.

For every desired boost curve, the pressure loop response must be shaped to preserve stability. This can be done with a pre-filter. To avoid unnecessary phase-shift, a faster valve, from a hydromechanical point of view, gives better flexibility to shape the pressure loop response with the pre-filter.

APPENDIX

Mechanical subsystem

The linearisation of equations (1) and (2) results in (17) and (18), neglecting friction for further linear analysis.

$$J_{sw}\theta_{sw}s^2 = T_{sw} - K_t\left(\theta_{sw} - R_tX_{rw}\right) - b_{rw}\theta_{sw}s \quad (17)$$
$$M_{rw}X_{rw}s^2 = P_LA_p + K_t\left(\theta_{sw} - R_tX_{rw}\right)R_t$$
$$- C_{rw}X_{rw} - b_{rw}X_{rw}s \quad (18)$$

The mechanical transfer functions are defined in (19) and (20).

$$G_{sw}(s) = \frac{1}{J_{sw}s^2 + b_{sw}s + K_t} \tag{19}$$

$$G_{rw}(s) = \frac{1}{M_{rw}s^2 + b_{rw}s + C_{rw} + K_t R_t^2} \tag{20}$$

Open-centre system

Linearising (3), (4), (6) and (7) results in (21) to (24), capital letters indicating linearised variables. K_q is the flow gain and K_c the flow-pressure coefficient.

$$Q_s = K_{q2}T_{sw} + K_{c1}P_s + K_{c2}P_l \tag{21}$$

$$Q_l = K_{q1}T_{sw} - K_{c2}P_s - K_{c1}P_l \tag{22}$$

$$Q_p - Q_s = \frac{V_s}{\beta}P_s s \tag{23}$$

$$Q_l = A_p X_p s + \frac{V_0}{\beta}P_l s \tag{24}$$

The derivatives are shown below, with w as the area gradient, which is used to rewrite the opening area as $A = wx_v$, and index 0 for operating points:

$$\frac{\partial q_s}{\partial T_{sw}} = C_q w_1 \sqrt{\frac{p_{s0} - p_{l0}}{\rho}} + C_q w_2 \sqrt{\frac{p_{s0} + p_{l0}}{\rho}} = K_{q2}$$

$$\frac{\partial q_s}{\partial p_s} = \frac{C_q T_{sw} w_1}{2\sqrt{\frac{p_{s0}-p_{l0}}{\rho}}\rho} + \frac{C_q T_{sw} w_2}{2\sqrt{\frac{p_{s0}+p_{l0}}{\rho}}\rho} = K_{c1}$$

$$\frac{\partial q_s}{\partial p_l} = -\frac{C_q T_{sw} w_1}{2\sqrt{\frac{p_{s0}-p_{l0}}{\rho}}\rho} + \frac{C_q T_{sw} w_2}{2\sqrt{\frac{p_{s0}+p_{l0}}{\rho}}\rho} = K_{c2}$$

$$\frac{\partial q_l}{\partial T_{sw}} = C_q w_1 \sqrt{\frac{p_{s0} - p_{l0}}{\rho}} - C_q w_2 \sqrt{\frac{p_{s0} + p_{l0}}{\rho}} = K_{q1}$$

$$\frac{\partial q_l}{\partial p_s} = \frac{C_q T_{sw} w_1}{2\sqrt{\frac{p_{s0}-p_{l0}}{\rho}}\rho} - \frac{C_q T_{sw} w_2}{2\sqrt{\frac{p_{s0}+p_{l0}}{\rho}}\rho} = -K_{c2}$$

$$\frac{\partial q_l}{\partial p_l} = -\frac{C_q T_{sw} w_1}{2\sqrt{\frac{p_{s0}-p_{l0}}{\rho}}\rho} - \frac{C_q T_{sw} w_2}{2\sqrt{\frac{p_{s0}+p_{l0}}{\rho}}\rho} = -K_{c1}$$

The coefficients for the pressure response, shown in (8), are defined as:

$$\omega_0 = \sqrt{\frac{K_{c1}^2 - K_{c2}^2}{V_0 V_s}\beta}$$

$$\delta_0 = \frac{1}{2}\frac{K_{c1}}{\sqrt{K_{c1}^2 - K_{c2}^2}}\frac{V_0 + V_s}{\sqrt{V_0 V_s}}$$

$$K_c = \frac{K_{c1}^2 - K_{c2}^2}{K_{c1}}$$

$$K_q = K_{q1}\left(1 + \frac{K_{q2}K_{c2}}{K_{q1}K_{c1}}\right)$$

Closed-centre system

The linearised equations for the closed-centre system are shown in (25) to (27), capital letters indicating linearised variables.

$$Q_{in} = K_{q1}X_{v_1} + K_{c_1}(P_s - P) \tag{25}$$

$$Q_{out} = K_{q2}X_{v_2} + K_{c_2}(P) \tag{26}$$

$$Q_{in} - Q_{out} = A_p X_p s + \frac{V}{\beta}P s \tag{27}$$

The meter-in and meter-out valves are controlled simultaneously as shown in (28). Equations (25) to (27) can be formed into (29), with $Q_l = A_p X_p s$ and hydraulic capacitance as $C_s = \frac{V}{\beta}$.

$$X_{v_2} = -X_{v_1} = -X_v \tag{28}$$

$$(K_{q_1} + K_{q_2})X_v + K_{c_1}P_s - Q_l =$$
$$(K_{c_1} + K_{c_2})P + \frac{V}{\beta}P s$$
$$\Rightarrow K_q X_v + Q_l = (K_c + C_s s)P \tag{29}$$

The derivatives are the following:

$$K_{q_1} = C_q w \sqrt{\frac{2}{\rho}(p_{s0} - p_0)} \tag{30}$$

$$K_{q_2} = C_q w \sqrt{\frac{2}{\rho}p_0} \tag{31}$$

$$K_{c_1} = \frac{C_q w x_{v_1 0}\sqrt{\frac{2}{\rho}}}{2\sqrt{(p_{s0} - p_0)}} \tag{32}$$

$$K_{c_2} = \frac{C_q w x_{v_2 0}\sqrt{\frac{2}{\rho}}}{2\sqrt{p_0}} \tag{33}$$

$$K_q = K_{q_1} + K_{q_2} \tag{34}$$

$$K_c = K_{c_1} + K_{c_2} \tag{35}$$

Parameter values

TABLE I
TABLE OF PARAMETER VALUES

Parameter	Value	Unit
J_{sw}	0.053	kgm^2
M_{rw}	30	kg
K_t	60.73	Nm/rad
R_t	154	rad/m
b_{sw}	0.23	Nm/s
b_{rw}	$1.05 \cdot 10^4$	Ns/m
C_{rw}	$3.86 \cdot 10^6$	N/m
A_p	$8.26 \cdot 10^{-4}$	m^2
V_p	$1.02 \cdot 10^{-4}$	m^3
C_q	0.67	-
ρ	850	kg/m^3
β	$8.7 \cdot 10^8$	Pa
q_p	9	l/min
F_f	0.3	Nm
ω_v	150	Hz
δ_v	0.7	-
w	$6 \cdot 10^{-5}$	m^2/U

REFERENCES

[1] A. Eidehall, J. Pohl, F. Gustavsson, and J. Ekmark, "Towards autonomous collision avoidance by steering," *IEEE Transactions on Intelligent Transportation Systems*, vol. 8, pp. 84–94, 2007.

[2] N. M. Enache, M. Netto, S. Mammar, and B. Lusetti, "Driver steering assistance for lane departure avoidance," *Control Engineering Practice*, vol. 17, pp. 624–651, 2009.

[3] G. Kovács, J. Bokor, L. Palkovics, L. Gianone, A. Semsey, and P. Széll, "Lane-departure detection and control system for commercial vehicles," in *IEEE International Conference on Intelligent Vehicles*, 1998.

[4] J. Ackermann and T. Bünte, "Yaw disturbance attenuation by robust decoupling of car steering," *Control Engineering Practice*, vol. 5, no. 8, pp. 1131 – 1136, 1997.

[5] J. Ackermann, "Active steering for better safety, handling and comfort," in *Proceedings of Advances in Vehicle Control and Safety*, 1998.

[6] K. Nam, H. Fujimoto, and Y. Hori, "Advanced motion control of electric vehicles based on robust lateral tire force control via active front steering," *IEEE/ASME Transactions on Mechatronics*, vol. 19, no. 1, pp. 289–299, February 2014.

[7] J. Tjønnås and T. A. Johansen, "Stabilization of automotive vehicles using active steering and adaptive brake control allocation," *IEEE Transaction on Control Systems Technology*, vol. 18, no. 3, pp. 545–558, May 2010.

[8] C. G. Keller, T. Dang, H. Fritz, A. Joos, C. Rabe, and D. M. Gavrila, "Active pedestrian safety by automatic braking and evasive steering," *IEEE Transactions on Intelligent Transportation Systems*, vol. 12, no. 4, pp. 1292–1304, December 2011.

[9] M. Tai, P. Hingwe, and M. Tomizuka, "Modeling and control of steering system of heavy vehicles for automated highway systems," *IEEE/ASME Transactions on Mechatronics*, vol. 9, pp. 609 – 618, December 2004.

[10] S. Haggag, D. Alstrom, S. Cetinkunt, and A. Egelja, "Modeling, control, and validation of an electro-hydraulic steer-by-wire system for articulated vehicle application," *IEEE/ASME Transactions on Mechatronics*, vol. 10, no. 6, pp. 688–692, December 2005.

[11] A. Bootz, M. Brander, and B. Stoffel, "Efficiency analysis of hydraulic power steering systems," in *The Eighth Scandinavian International Conference on Fluid Power, SICFP'03*, Tampere, Finland, 2003.

[12] A. Balachandran and J. C. Gerdes, "Desdesign steering feel for steer-by-wire vehicles using objective measures," *IEEE/ASME Transactions on Mechatronics*, 2014.

[13] J. E. Forbes, S. M. Baird, and T. W. Weisgerber, "Electrohydraulic power steering - an advanced system for unique applications," in *SAE International Congress and Exposition*, no. 870574, Detroit, Michigan, USA, 23-27 February 1987.

[14] J. Gessat, "Electrically powered hydraulic steering systems for light commercial vehiclesc," in *SAE 2007 Commercial Vehicle Engineering Congress and Exhibition*, no. 2007-01-4197, 2007.

[15] A. Badawy, D. Fehlings, A. Wiertz, and J. Gessat, "Development of a new concept of electrically powered hydraulic steering," in *SAE 2004 Automotive Dynamics, Stability and Control Conference and Exhibition*, no. 2004-01-2070, 2004.

[16] R. McCann and A. Le, "Gain scheduling in commercial vehicles with electrohydraulic power steering," in *SAE Commercial Vehicle Engineering Congress and Exhibition*, no. 2008-01-2703, 2008.

[17] K. Suzuki, Y. Inaguma, and K. H. abd Tomomi Nakayama, "Integrated electro-hydraulic power steering system with low electric energy consumption," in *SAE International Congress and Exposition*, no. 950580, 1995.

[18] Y. Inaguma, K. Suzuki, and K. Haga, "An energy saving technique in an electro-hydraulic power steering (ehps) system," in *SAE International Congress and Exposition*, no. 960934, 1996.

[19] A. Badawy, J. Zuraski, F. Bolourchi, and A. Chandy, "Modeling and analysis of an electric power steering system," in *SAE International Congress and Exposition, Steering and Suspension Technology Symposium*, no. 1999-01-0399, Detroit, Michigan, March 1999.

[20] M. Wellenzohn, "Improved fuel consumption through steering assist with power on demand," in *SAE Convergence 2008*, no. 2008-21-0046, 2008.

[21] C. Morton, V. Pickert, and M. Armstrong, "Self-alignment torque as a source of energy recovery for hybrid eletric trucks," *IEEE Transactions on Vehicular Systems*, vol. 63, no. 1, pp. 62–71, January 2014.

[22] P. Koehn and M. Eckrich, "Active steering - the bmw approach towards modern steering technology," in *SAE Steering and Suspension Technology Symposium*, no. 2004-01-1105, Detroit, Michigan, USA, 2004.

[23] M. Rösth, J. Pohl, and J.-O. Palmberg, "Active pinion - a cost effective solution for enabling steering intervention in road vehicles," in *The Bath Workshop on Power Transmission & Motion Control, PTMC'03*, Bath, United Kingdom, September 2003.

[24] U. Wiesel, A. Schwarzhaupt, S. Gast, J. Wirnitzer, M. Frey, and F. Gauterin, "A method for evaluating the fuel saving potential of different hybrid steering system configurations in heavy vehicles," in *VDI-Berichte 2068*, 2009.

[25] S. Müller, A. Kugi, and W. Kemmetmüller, "Analysis of a closed-center hydraulic power steering system for full steer-by-wire functionality and low fuel consumption," in *The Ninth Scandinavian International Conference on Fluid Power, SICFP'052*, 2005.

[26] W. Kemmetmüller, S. Müller, and A. Kugi, "Mathematical modeling and nonlinear controller design for a novel electrohydraulic power-steering system," *IEEE/ASME Transactions on Mechatronics*, vol. 12, no. 1, pp. 85 – 97, February 2007.

[27] A. Bootz, "Evolutionary energy saving concepts for hydraulic power steering systems," in *5th International Fluid Power Conference*, 2006.

[28] P. E. Pfeffer, "Interaction of vehicle and steering system regarding on-center handling," Ph.D. dissertation, Deparment of Mechanical Engineering, University of Bath, 2006.

[29] M. Rösth, "Hydraulic power steering system design in road vehicles; analysis, testing and enhanced functionality," Ph.D. dissertation, Division of Fluid and Mechanical Engineering Systems, Linköping University, 2007.

[30] J. Post and E. Law, "Modeling, characterization and simulation of automobile power steering systems for the prediction of on-center handling," in *SAE International Congress & Exposition*, no. 1996-02-01, February 1996.

[31] A. Zaremba and R. Davis, "Dynamic analysis and stability of a power assist steering system," in *Proceedings of the American Control Conference*, Seattle, Washington, June 1995.

[32] E. Ueda, E. Inoue, Y. Sakai, M. Hasegawa, H. Takai, and S. Kimoto, "The development of detailed steering model for on-center handling simulation," in *International Symposium on Advanced Vehicle Control (AVEC)*, 2002, pp. 657 – 662.

[33] A. Dell'Amico, "Pressure control in hydraulic power steering systems," 2013, lic. thesis No. 1626, Linköping University.

[34] M. Rösth and J.-O. Palmberg, "Robust design of power steering system with emphasis on chattering phenomena," in *The 10th Scandinavian International Conference on Fluid Power, SICFP'07*, 2007.

[35] H. E. Merritt, *Hydraulic Control Systems*. John Wiley & Sons, USA, 1967.

[36] C. Ramdén, "Experimental methods in valve characteristic assessment," Ph.D. dissertation, Linköping University, 1999.

[37] M. Sannelius, "On complex hydrostatic transmissions," Ph.D. dissertation, Linköping University, 1999.

[38] D. Auslander, "Distributed system simulation with bilateral delay-line models," *Journal of Fluids Engineering*, vol. 90, no. 2, pp. 195–200, June 1968.

Alessandro Dell'Amico received his Master of Science in Mechanical Engineering from Linköping University and is currently working towards a PhD degree at the division of Fluid and Mechatronic Systems, Linköping University. Research interest in modelling, simulation and control of fluid power systems, mechatronic systems and digital hydraulics. Applications are in automotive systems and construction machinery.

Petter Krus Professor in Fluid and Mechatronic Systems at Linköping University. Research interest in fluid power, mechanical, and mechatronic systems technology, specifically focusing on system dynamics, control, system simulation, optimization, system design and design automation. Applications are in aircraft design, road vehicles and construction machines.